J Mater Sci: Mater Med (2008) 19:3443–3453
DOI 10.1007/s10856-008-3487-1

An electrochemical impedance investigation of the behaviour of anodically oxidised titanium in human plasma and cognate fluids, relevant to dental applications

B. Bozzini · P. Carlino · L. D'Urzo · V. Pepe · C. Mele · F. Venturo

Received: 2 April 2007 / Accepted: 23 May 2008 / Published online: 27 June 2008
© Springer Science+Business Media, LLC 2008

Abstract In dental applications, the contact between the metal implant and the receiving living tissue is made through the oxide layer on the implant surface, which allows the osseointegration process. In dentistry, the passive film formed on titanium seems to be more stable and protective than that formed on the Ti alloys, customarily used in other medical applications. Corrosion of titanium alloys in the mouth can result from the presence of a number of corrosive species, such as the hydrogen ion (H^+), sulfide compounds (S^{2-}), dissolved oxygen (O_2) and Cl^- and can result in the release of Ti^{4+} ions that, in turn, brings about the reduction of alkaline phosphatase activity of osteoblastic cells. The present study reports a time-dependent electrochemical corrosion study of titanium in contact with the following biologically relevant solutions: (i) SBF (simulating the inorganic part of human plasma), (ii) SBF with added ovalbumin (a protein simulating the post-implant environment) and (iii) human plasma. To the best of the authors' knowledge, this is the first report on the corrosion of Ti in human plasma. The electrochemical measurements are based on electrochemical impedance spectrometry. Impedance spectra were interpreted on the basis of the equivalent-circuit approach and estimates of the time-variation of oxide film thickness and resistance were computed. Surface Raman spectroscopy was used to characterise the structure of as-anodised and corroded TiO_2 films: the effects of phosphate and organic incorporation were highlighted. EIS and surface Raman measurements have demonstrated that the corrosion resistance of the oxide films formed on Ti is strongly affected by the presence of biomolecules in the chloride- and phosphate-based aqueous solution. In particular, ovalbumin increases corrosion performance and human plasma is found to be remarkably more aggressive in comparison to SBF. These results suggest some caution in extrapolating corrosion results obtained in simulated biological fluids to the actual behaviour in vivo.

B. Bozzini (✉) · L. D'Urzo · C. Mele
Dipartimento di Ingegneria dell'Innovazione,
Università di Lecce, via Monteroni, 73100 Lecce, Italy
e-mail: benedetto.bozzini@unile.it

P. Carlino · V. Pepe · F. Venturo
Dipartimento di Odontostomatologia e Chirurgia, Università
di Bari, piazza Giulio Cesare, 70124 Bari, Italy

1 Introduction

Nowadays, osseointegrated dental implants can be regarded as well-proven safe devices, which are routinely used on a large scale in order to functionally rehabilitate both partially and totally edentulous patients. One of the chief success factors of modern osseointegrated dental implants is related to the achievement of a fast and tight interconnection between the implant surface and bone tissue [1–4].

As far as dentistry is concerned, the essential features of titanium are: (i) very low density (a factor of four less than that of gold); (ii) relatively low thermal conductivity (a factor of 14 times lower than that of gold); (iii) elasticity modulus close to that of bone tissue. These peculiarities allow the tolerance of the mechanical loads related to chewing—that are transferred to the bone tissue through the implant device—without the development of potentially critical stresses. Furthermore, titanium exhibits other optimal characteristics such as: (i) outstanding level of biocompatibility, (ii) remarkable corrosion resistance (iii) comparatively high hardness, (iv) it is a-magnetic, (v) it exhibits a low coefficient of thermal expansion. These

conditions are, of course, essential to the success of osseointegration that crucially depends also on the implant-tissue bone integration and respective biological, chemical and mechanical stability as well as lack of interaction with stray or medically relevant electromagnetic fields. The high corrosion resistance of titanium depends on the physico-chemical properties of the oxide layer—exhibiting typically a nanometric thickness—forming on its surface upon exposure to many aerated aqueous environments. Such oxide films are often highly homogeneous, tough and adherent, furthermore they are essentially inert from the chemical and biological standpoints, extremely homogeneous, and adherent; furthermore, its bacteriostatic activity has been demonstrated [1, 2].

The film, that tends to form also spontaneously by exposure to humid air, can be readily modified by chemical and electrochemical techniques, typically by anodic oxidation. The controlled anodic oxidation of titanium exhibits two major points of interest for biomedical applications, related to the possibility of growing: (i) compact high-thickness films, apt at maximising the corrosion resistance and improving the biocompatibility of the implant; (ii) porous films incorporating Ca^{2+} and PO_4^{3+}, able to enhance osseointegration [1–3, 5–7].

The interaction of proteins with the TiO_2 surface is dominated by the electrostatic forces: (i) between amino acid groups bearing positive charges ($–NH_3^+$) and the negatively charged TiO_2; (ii) between carboxylic groups with negative charge ($–COO^-$) through the bridging action of Ca^{2+} ions adsorbed on the negatively charged TiO_2 surface. Moreover, direct bonding of $–COO^-$ groups to titanium cations is possible, going on through the substitution of hydroxyl groups [5, 6, 8].

When the titanium implant is inserted into the human body, blood components—in particular the serum proteins—lipoproteins and peptides, can affect the implant corrosion. Furthermore, inorganic species present in the biological fluids, such as calcium and phosphate ions can be adsorbed or even incorporated into the TiO_2 layer, evolving during exposure to the biological environment. Corrosion of Ti implants is critical, because it can adversely affect both biocompatibility [5–7] and mechanical performances [8–13]. Furthermore, the presence of titanium corrosion products has been correlated with the reduction of the rate of production of the bone matrix by osteoblastic cells [8–13]. For this reason, studies of the corrosion of titanium and some of its alloys have been performed in a variety of media simulating human fluids [7, 14–24].

Passive films have been shown by electrochemical impedance spectrometry (EIS) to form in phosphate buffer solution, but to dissolve in artificial saliva [22]. Moreover, the properties of the oxide film present on titanium implants are believed to play an important role during the osseointegration process [1–3]. Direct EIS measurements on dental screws have also been reported [22]. The corrosion has been studied of titanium, subjected to the mechanical surface treatments customarily used for the controlled roughening of commercial implants [7]. The key facts relating to Ti corrosion in the relevant case are growth and dissolution of the TiO_2 layer, changing the properties of the optimal pre-formed TiO_2 layer. Since the success of titanium implants relies heavily on the long-term stability of TiO_2 in biological environments, it is highly desirable to monitor its electrochemical behaviour and to induce structural and functional information from it. The passive film formed by anodisation or chemical treatments on Ti and its alloys is mainly amorphous TiO_2 [25, 26], but—especially at higher thicknesses [25] or under special electrochemical conditions [27–30] crystalline layers can be obtained; its electronic behaviour is that of a highly doped n-type semiconductor [31, 32]. High anodic polarisations bring about the transformation of semiconducting TiO_2 into TiO(OH), exhibiting electronic conductivity [33]. The precipitation of hydrates might exhibit a sealing activity with respect to the outer porous oxide layers. The passive films formed on pure (typically 99.99%) Ti seems to be more stable and protective than those formed on some Ti alloys (open-circuit (OC) data in phosphate buffer solution have been reported in [23, 34]). The instability of the oxide film has been related to the interstitial elements present in the alloy [22]. Pan proved that the addition of H_2O_2 to a phosphate buffer solution caused a remarkable decrease of the corrosion resistance of Ti and a thickening of the porous outer layer [14].

As far as the mechanism of TiO_2 dissolution is concerned, chemical dissolution of the oxide film ought to be taken into account as well as electrochemical oxidation of Ti, since—both at OC [35] and under anodic polarisation conditions [21]—the rate of oxide layer formation is in competition with its removal at the metal/solution interface; of course the chemical details of the biological solution are vital in this respect. Moreover, it has been proved that the surface film formed on Ti implants in a human body, after some years can reach thicknesses far in excess of the nm-range and that mineral ions can end up incorporated in the oxide film [36].

In this paper an EIS and surface Raman study is described, concerning the influence of the environment on the long-term stability of pre-grown TiO_2 layers formed onto Ti under electrochemical control. Similar experiments, though carried out with TiO_2 films grown in a different way and exposed to different environments, are reported in the literature, based on EIS at OC: (i) in phosphate buffer for ca. 30 days [14], (ii) in F^--containing aqueous solutions, for ca. 1 day [20] and for ca. 2 weeks

[18], (iii) in artificial saliva for ca. 1 day [22] and ca. 7 days [23]. The aim of this work is to assess the corrosion resistance of titanium in contact with human plasma. Since the chemistry of this system is extremely entangled, with many different components potentially affecting the interfacial electrochemistry and oxide stability, we carried out measurements both in the real plasma and in two synthetic solution, able to stress the effect of some of the key components, namely: (i) the inorganic aqueous matrix, represented by SBF (simulating the inorganic content of human biological fluids); (ii) SFB containing OVA, a protein commonly used in the literature [37, 38] and references therein contained) in order to simulate the behaviour of albumin, the single protein exhibiting the highest surface coverage of the implant during the initial stages of the healing process; (iii) the full human plasma.

2 Materials and methods

Ti foils were employed of thickness 2 mm and purity 99.7%. The Ti samples were etched in an aqueous solution of composition: 60% HNO_3, 40% HF and water in the ratios 15:10:75. The etched samples were anodised in 0.5 M H_2SO_4 with the following procedure: a conventional three-electrode configuration was used with an AMEL 7050 potentiostat, a potential of −1 V versus Ag/AgCl was initially applied and it was scanned linearly at a sweep rate of 2 mV s^{-1} up to 2 V. Anodisation rates for the relevant TiO_2 growth conditions are reported to lie in the range 2.5–3.25 nm V^{-1} [18, 34, 39], no attempts were made to directly measure the thickness oxide layers grown in this research. The choice of the anodising conditions corresponds to a thickness in the range relevant to dental applications [2–4].

The measurements were carried out with the following solutions at pH 6.9 ± 0.1.

(i) SBF: NaCl 20.2 g l^{-1}, $NaHCO_3$: 0.483 g l^{-1}, Na_2SO_4: 0.104 g l^{-1}, Na_2HPO_4: 0.411 g l^{-1}, KCl: 0.716 g l^{-1}, $CaCl_2$: 0.433 g l^{-1}, $MgCl_2$: 0.381 g l^{-1}, pH 6.9 [40].
(ii) SBF + OVA: 40 g l^{-1} of ovalbumin (EGR B6, Riedel-De Heän AG) (henceforward OVA) were added to the SBF solution, described above.
(iii) The human plasma had a specific weight of 1,027–1,030 g l^{-1}, and a pH 7.3–7.4. The plasma composition is given in Table 1.

In use in this work, the human plasma was obtained from a pool of biologically healthy volunteers with hematic standard values and treated with EDTA, in order to inhibit the coagulation process. Within one hour after extraction, the sample was purified from red cells and cellular fragments by centrifugation at 1,550*g* for 30 min. The whole sample was divided into 5 aliquots, that were frozen at a temperature of ca. −30°C. During the experimental time (5 days), one aliquot of plasma was unfrozen per day and used for electrochemical measurements.

Table 1 Composition of the human plasma employed in this investigation, balance: water. The reported figures express the average and standard deviation among the five collected plasma samples

Proteins
Albumin 59.1 ± 4.3%,
Globulins
Alpha1 4.3 ± 1.1%
Alpha2 9.4 ± 1.3%
Beta1 6.3 ± 0.8%
Beta2 4.9 ± 1.5%
Gamma 16.0 ± 2.1%
Fibrinogen 313 ± 77 mg/dl
Organic components
Bilirubin 0.43 ± 0.25 mg/dl
Glucose 81 ± 5 mg/dl
Urea 32 ± 3 mg/dl
Creatinine 0.7 ± 0.05 mg/dl
Cholesterol 158 ± 22 mg/dl
Triglycerides 43 ± 11 mg/dl
Inorganic components
Na^+, K^+, Ca^+, Cl^-, HCO_3^-, HPO_4^-, Fe^{2+}, I^-) 0.90 ± 0.05%
Hormones, enzymes, vitamins, antibodies: traces

EIS experiments were carried out with an AMEL 5000 potentiostat connected to a frequency response analyser (Solartron SI 1250) in the frequency range 65 kHz to 1 mHz with voltage modulation of amplitude 10 mV peak-to-peak. The measurements were performed at room temperature, using a three-electrode cell holding 75 ml of electrolyte. An Ag/AgCl reference electrode was used and all potentials are quoted on the Ag/AgCl scale. The counter-electrode was a platinised Ti expanded mesh electrode of nominal area 10 cm^2. In all experiments, apart from those carried out with plasma, between subsequent EIS measurements the samples were kept immersed in sealed vessels containing 150 ml of the relevant aerated solutions. The EIS spectra were fitted with a suitable equivalent-circuit model, described in Sect. 3, with the Z-view software (SCRIBNER ASSOCIATES INC).

LSV measurements were run in the potential interval OC-1,200 mV versus Ag/AgCl at a scan rate of 2 mV s^{-1}, an anodised Ti sample in contact with the SBF solution. In Fig. 1 we report the LSV plot, exhibiting very low cds, indicative of the fact that the investigated potentials lie within the passive range.

Surface Raman measurements were carried out with a Raman microprobe system (LabRam Jobin-Yvon) equipped with a confocal microscope, CCD detector, interferometric

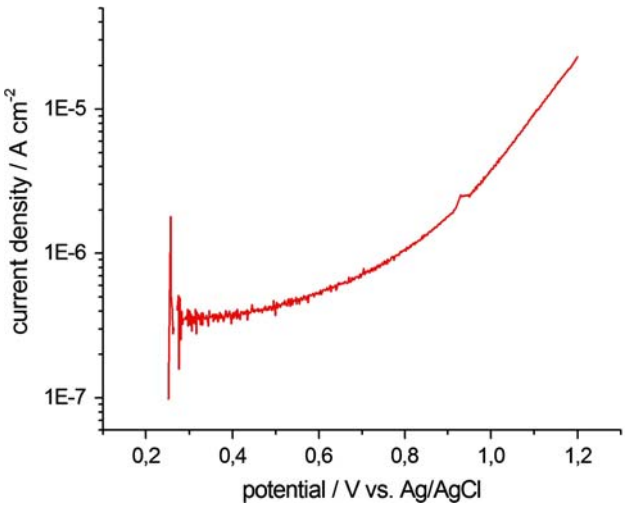

Fig. 1 Linear sweep voltammetries of anodised Ti sample in SBF solution. Scan rate: 2 mV s^{-1}

and holographic notch filters and 50× long-working-distance objective. A He–Ne laser provided the excitation at 632.8 nm and the power delivered to the sample was about 7 mW.

2.1 Electrochemical methods

In the interpretation of impedance data, models based on those of [7, 14, 41–45] were used. The literature models essentially represent the dynamic behaviour of compact single layers or double layers comprising a compact and a porous part. In the case of single layer models, the capacitance of the compact layer can be used to estimate its thickness. A caveat is nevertheless necessary. In [44] it has been proved that the capacitive behaviour of the interface *Ti/TiO$_2$/electrolyte*, as measured by EIS, can be markedly influenced by the space-charge region, corresponding to the thin, compact inner layer of the actual duplex structure of TiO_2 layers grown onto Ti [14, 21, 39, 46]; the dissolution rate of the outer layer was found to be about the double of that of the inner one. It is thus highly recommended to take this factor into account when endeavouring to estimate the TiO_2 thickness from EIS data, especially when small-field measurement conditions prevail (such as at OC) and for pre-formed TiO_2 grown by the high-field mechanism. In terms of equivalent circuit, this contribution amounts to adding an RC parallel accounting for the contribution of the space charge-layer, the additional parameters are: R_{SC} [Ω cm^2]: the resistance of the space-charge region; C_{SC} [F cm^{-2}]: the capacitance of the space-charge region. C_{SC} can be estimated by running EIS experiments at various potentials within the passive region, estimated e.g. by linear sweep voltammetry (LSV), and drawing a Mott–Schottky plot:

$$C_{SC}^{-2}(E) = 2\frac{E - E_{FB} - \frac{kT}{e}}{N_D \varepsilon \varepsilon_o e} \quad (1)$$

where E [V] is the applied potential; E_{FB} [V] is the flat-band potential; k [J K^{-1} C^{-1}] is the Boltzmann constant; T [K] is the absolute temperature; e [C] is the electron charge; and N_D [mol cm^{-3}] is the donor concentration (typically Ti^{3+} trapped in the process of migrating to the oxide/electrolyte interface [47]).

ε [a dimensional] is the material relative dielectric constant and ε_o [F mol cm^{-3}] is the vacuum dielectric constant. In this context, N_D and E_{FB} can be regarded as fit parameters. A selection of accurately derived values for these quantities is available in [18] and references therein contained.

With these considerations in mind, the simplest equivalent circuit able to account for the observed spectra as well as space-charge requirements, is an RC parallel, with C_P [F cm^{-2}]: the capacitance of the passive film and R_{SC}. A more insightful discussion of this point is reported in Sect. 4.1.2 below. The reciprocal of C_P is directly proportional to the compact oxide layer thickness d [16]:

$$d = \frac{\varepsilon \varepsilon_o A}{C_P} \quad (2)$$

where ε is the relative dielectric constant of the oxide, ε_o that of vacuum and A is the oxide layer surface area; since roughening is vanishing in this case—as assessed by scanning electron microscopy observations not reported for brevity—the geometric surface area of the electrode is a good value In the relevant case, expressing d in nm, C_P in μF and A in cm^2, it results that: $\varepsilon\varepsilon_o$ = 47.32 μF nm^{-1}.

Non-linear least-squares fits of all data sets were carried and model selection was performed on the basis of the values of the chi-square $\chi^2$and linear correlation coefficient ρ^2; further relevant details are provided in Sect. 3.

3 Results and discussion

3.1 Characterisation of Ti oxide films

3.1.1 Linear sweep voltammetry (LSV)

Typical LSV curves for cognate systems have been reported in [18, 20, 21, 44]. The current densities (cds) are low in the passive region, extending over a wide potential range. A passivation peak was found in artificial saliva containing F^- [18, 20] or after high anodic prepolarisation [23]. In the absence of F^-, a difference was found between the zero-current potential in the forwards and backwards scans, that was explained with the formation of a barrier layer [20]. LSVs were also measured on dental screws, yielding essentially the same results as with Ti disks [22].

3.1.2 *Mott–Schottky analysis and discussion of the impedance model*

In order to carry out a Mott–Schottky analysis for the evaluation of C_{SC}, we run EIS measurements at a series of fixed potentials within the passive range, we fitted the relevant spectra with the model recommended in [48] and elaborated the thereby estimated parameters with Eq. 1, eventually producing Mott–Schottky plots, from which the parameters E_{FB} and N_D, controlling the space-charge capacitance contribution C_{SC}, can be estimated. The potentials considered were between 200 and 1,200 mV and were sampled in steps of 200 mV. The results of the Mott–Schottky analysis are reported in Fig. 2. From the results reported in Fig. 2 it can be noticed that relatively high C_{SC} values are found, in comparison with results obtained with samples anodised at higher voltages, denoting a smaller contribution of the space-charge region to the total electrode capacitance. If the oxide layer is grown before exposing the sample to the aggressive environment, the properties of the space-charge region can be regarded as an intrinsic material property of the Ti/TiO_2 system (see Sect. 2.1) and—in order to assess the contribution of C_{SC} to the estimation of the oxide thickness—it is not necessary to carry out Mott–Schottky analyses in all the electrolytes considered.

In the particular case at hand, the impact of employing an *additional parallel* including C_{SC} seems very minor in the quantitative analysis of the measured impedance spectra (i.e. a specific loop could not be measured in the frequency range investigated, it might have appeared if higher frequencies had been considered, but this measurement is not possible with the instrument available to this group) and eventually in the evaluation of the passive

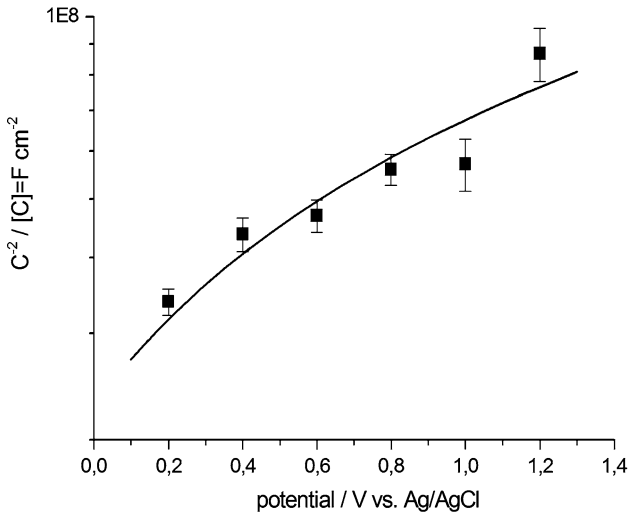

Fig. 2 Mott–Schottky plots for the anodised Ti sample in SBF solution

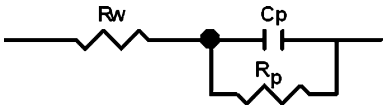

Fig. 3 The equivalent-circuit model selected for the interpretation of electrochemical impedance spectra measured in this work. R_W is the Warburg impedance, R_P and C_P are the charge-transfer resistance and the capacity of the inner compact passive layer

layer thickness and resistance. In [14] it has been pinpointed that the detailed impedance behaviour of the relevant system derives from three regions of the interface: the space charge region, the inner compact passivating layer and the outer porous layer. The relative values of the electric parameters describing the impedance corresponding to the three above-mentioned regions, together with the fact that the corrosion behaviour is dominated by the compact passivating layer and that the space-charge region is essentially constant in our experiments, led us to develop an approximate equivalent-circuit model that highlights the effect of the passivating layer itself. Elaborating on the network corresponding to the model including both the effects of the porous and space-charge layers, boils down to the model shown in Fig. 3. Of course, this crude model eventually boiled down to handling the multilayer modified oxide layer, possibly containing incorporated ions or even proteins and probably coated with a protein film, in an integral way as a single object described by two parameters. Nevertheless, the authors reckon that this approach is highly recommendable—especially if it comes to detecting changes of corrosion behaviour with environment and time and to ranking materials—because an increase of model details would be taxed by a dramatic decrease of the reliability, relevance and diagnosticity of the estimated parameters.

3.2 Time-dependent electrochemical impedance spectrometry (EIS) measurements at open-circuit (OC)

EIS measurements at OC of Ti and its alloys have been described in the literature [16, 20, 22]: essentially four kinds of spectral behaviour were found.

(i) One or two depressed semicircles, sometimes accompanied by a diffusion tail. This kind of behaviour indicates that charge-transfer reactions are active, the diffusion signature might denote either the fact that high charge-transfer rates are achieved or that corrosion goes on through an interfacial layer; model discrimination is possible on the basis of polarisation resistance values [16, 20, 48]. The presence of two time constants has been also interpreted in terms of the formation of a two-layer oxide film [21, 48].

(ii) Pure capacitive behaviour over a wide frequency range, indicating the presence of a compact passive film and therefore denoting a high corrosion resistance [16].

(iii) Only an arc of a semicircle can be measured in the accessible frequency range. In this case the response is nearly capacitive, but some slow charge-transfer reaction is taking place: this spectral behaviour is typical of a passive oxide film [7, 14, 16, 21, 22, 49]. Owing to the incompleteness of the circle, in this particular case special attention should be devoted to the numerical estimation of the model parameters. In this instance, working with the Bode plot might be recommendable, since a clear-cut spectral behaviour is found: (a) the logarithm of the impedance modulus is essentially linear with the logarithm of frequency, with a slope of ca. 1 and (b) the phase angle values tend to approach 90° (ca. 80° in most of the practical cases).

From the literature, typical C_P values are found in the range 5–40 μF cm^{-2} [14, 16, 21, 22]; such relatively low values have been interpreted as indicative of the long-term stability of the passive film. A slight decrease of capacitance in phosphate buffer solution has been explained with a slow growth of the TiO_2 layer [14].

R_P values of ca. 2 [16] and 5 [14] MΩ cm^2 have been considered to be high enough to correlate with high corrosion resistance. Values of 5 MΩ cm^2, decreasing to 1 MΩ cm^2 after 24 h of exposure to the aggressive environment have been found with a dental screw; such time dependence has been interpreted as due to the partial dissolution of the oxide barrier layer [22]. R_P values in the range 13–540 kΩ cm^2 were reported in [21], referring to a Ti–Al–Nb alloy in Hank's solution; in this case, the decrease of resistance with increasing anodic polarisation has been correlated to a increase of the oxide defectivity. The resistance increase, observed in [14] has been explained with a re-growth of the inner layer or to a self-healing phenomenon. Capacitance and resistance values (that can be interpreted as C_P and R_{SC}, respectively, according to the model shown in Fig. 3) have been found to increase and decrease, respectively with immersion time in F^--containing solutions. Values of the CPE parameter n have been found in the range 0.50–0.95 [18, 21, 50], in some cases this parameter has been held fixed during NLLS fitting.

In order to evaluate the stability of the *Ti/TiO$_2$/electrolyte* interface in contact with different aerated electrolytes relevant to dental implant applications, we have kept our samples continuously immersed in the respective solutions and carried out EIS measurements discontinuously. The EIS spectra contained in the various data sets measured with Ti samples and electrolytes, were fitted by NLLS with the equivalent-circuit models discussed in Sect. 2.1 (Electrochemical methods) and the results of these fits were compared on the basis of their statistical characteristics. Out of a set of alternative models—not described here for the sake of brevity (for relevant details, see e.g. [51, 52])—we selected Fig. 3 for the following reasons: (i) all qualitative features of the impedance spectra can be captured, (ii) lower confidence intervals for the parameter estimates are obtained, (iii) less correlated parameters are estimated. The linear correlation coefficients corresponding to the NLLS fits are reported in Table 2 from this model, the following two parameters—diagnostic of the environmental stability of the interface—could be extracted: the passive film resistance R_p and the film capacitance C_p. The NLLS estimates of these parameters and their 95% confidence intervals are employed in the discussion of our electrochemical corrosion measurements. The film capacitance values—accounting for space-charge effects after the results of our Mott–Schottky analysis, according to the procedure recommended in [44]—were converted into film thickness with Eq. 2. The confidence intervals for the

Table 2 ρ^2 values for the different NLLS fits performed in this work

Electrolyte investigated	Figure #	Immersion time (days)	ρ^2
SBF	4	0	0.9722
SBF	4	1	0.9808
SBF	4	4	0.9896
SBF	4	5	0.9961
SBF	4	6	0.9869
SBF	4	15	0.9588
SBF	4	19	0.9703
SBF	4	29	0.9968
SBF	4	34	0.9958
SBF + OVA	8	0	0.9705
SBF + OVA	8	1	0.9947
SBF + OVA	8	4	0.9529
SBF + OVA	8	5	0.9676
SBF + OVA	8	6	0.9907
SBF + OVA	8	15	0.9505
SBF + OVA	8	19	0.9569
SBF + OVA	8	29	0.9601
SBF + OVA	8	34	0.9599
Plasma	9	0	0.9802
Plasma	9	0.96	0.9636
Plasma	9	1.04	0.9599
Plasma	9	1.8	0.9508
Plasma	9	2.6	0.9873

film thickness were computed according to [53]. Of course, the absolute thickness values ought to be taken as indicative and their meaning is essentially a comparative one, because this is an indirect estimate going through multiplication by dielectric constants that have been assumed to be equal to that of water for the different electrolytes and numerically deriving from the reciprocal of a relatively large quantity with some—though controlled (via the confidence interval estimate)—statistical uncertainties.

3.2.1 *The system Ti/SBF*

In Fig. 4 we report the EIS spectra of anodised Ti in contact with the SBF solution, measured over a period of 28 days. The evolution of the OC potential (OCP) as a function of time—exhibiting a slight progressive ennobling (−120 to +250 mV)—is shown in Fig. 5a (the line through the data is only a guide for the eye). The estimates of time-dependent passive film thickness d and resistance R_p are reported in Figs. 6a and 7a. An approximately linear increase in d (ca. 2–15 nm) and an approximately exponential decrease in R_p (ca. two orders of magnitude, starting from 1.4 MΩ cm^2) were found. These trends, in particular the ennobling of OC—indicating a more active state for the underlying metal—and the decrease of R_P)—correlating with a higher passivity corrosion current density—, denote a progressive degradation of the corrosion resistance of the Ti/TiO_2 interface: the film thickness tends to increase, but its protective capability gets degraded with exposure time.

Of course, the structure and chemistry of the interfacial TiO_2-related compounds is very complex and—on the basis of the data available—it is hard to draw definitive mechanistic conclusions. The electrochemical evidence hints at the development of a modified, thicker passivating film with a higher charge-transfer capability, the assessment of whose nature (see e.g. [54]) would require specific studies beyond the scope of this paper. The Surface Raman spectra (see Sect. 3.3) corresponding to these experimental conditions highlight the presence of phosphate in the otherwise unmodified initial rutile structure. One expects these ions to reside in the porous outer layer rather than in the compact inner layer (see Sect. 3.3 for details), but our simple—but robust (see Sects. 3.1.2 and 3.2)— impedance model is not able to discriminate between these two regions.

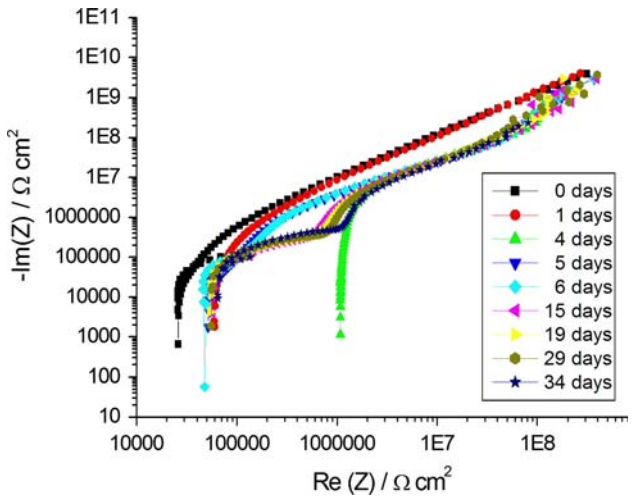

Fig. 4 EIS spectra of anodised Ti in contact with the SBF solution

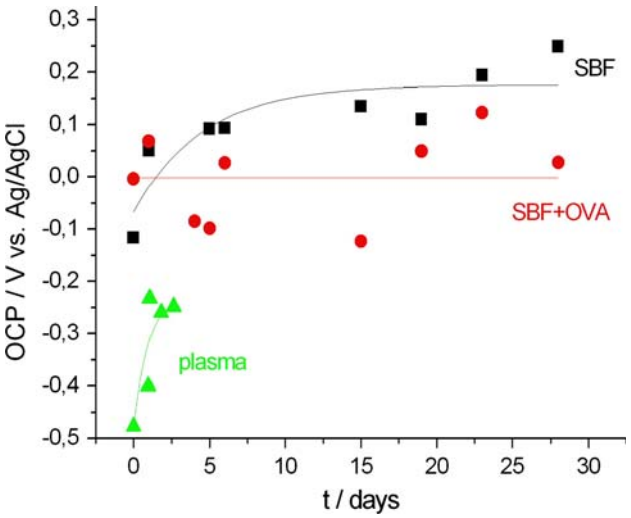

Fig. 5 OCP of anodised Ti in contact with the following solutions: SBF, SBF solution containing OVA, plasma

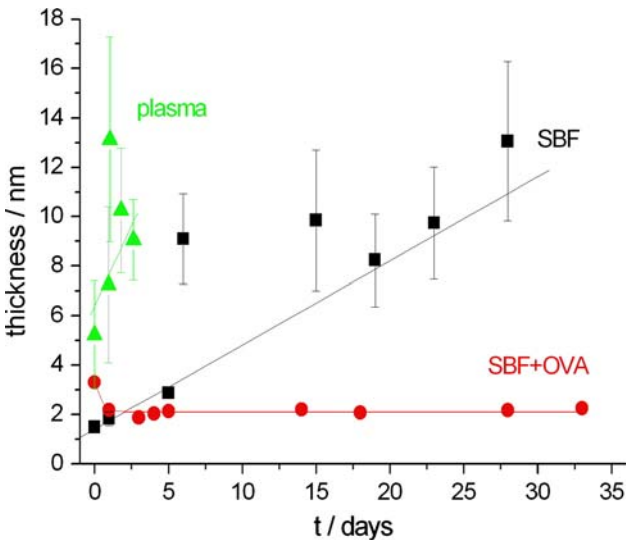

Fig. 6 Estimate of the time-dependent passive film thickness for anodised Ti in contact with the following solutions: SBF, SBF solution containing OVA, plasma

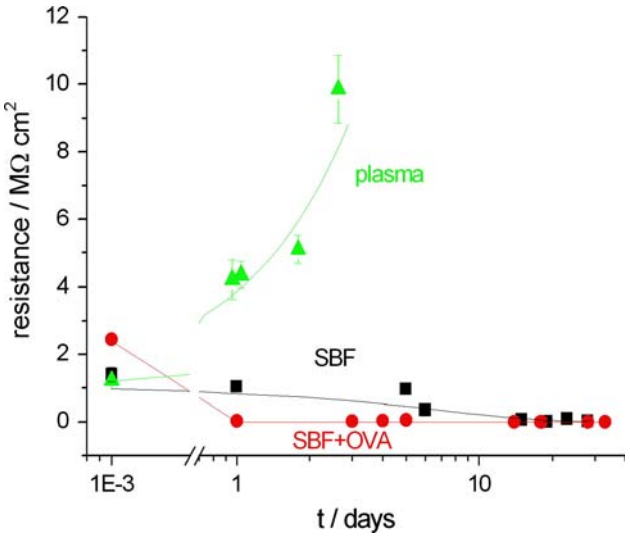

Fig. 7 Estimate of the time-dependent passive film resistance for anodised Ti in contact with the following solutions: SBF, SBF solution containing OVA, plasma

3.2.2 *The system Ti/SBF + OVA*

In Fig. 8 we report the EIS spectra of anodised Ti in contact with the OVA-containing SBF solution, measured over a period of 33 days. The OCP as a function of time are shown in Fig. 5b; no clear-cut evolution can be noticed and the OCP seems to fluctuate around a value of ca. 0 mV. The estimates of time-dependent passive film thickness d and resistance R_p are reported in Figs. 6b and 7b. An immediate, slight decrease in d (ca. 3–2 nm) is noticed, followed by an essentially constant value and a faster than exponential decrease in R_p (from ca. 2 MΩ cm^2 to ca. 3 kΩ cm^2). The high initial thickness values can be related to OVA adsorption, coherently with our surface Raman results reported and discussed in Sect. 3.3. Also in this case a progressive degradation of the corrosion resistance of the Ti/TiO_2 interface is found, but the presence of OVA seems to correlate with different processes; in fact, d decreases, but the R_p, though decreasing, seems to tend towards a higher asymptotic value than in the absence of OVA. OVA seems to provide some degree of corrosion-inhibiting activity to the Ti/TiO_2 interface in the aerated SBF solution. As stressed in Sect. 3.1.2, our EIS model does not allow us to follow explicitly the adsorption processes that are most probably related to the presence of OVA (see, e.g. [55]). Therefore the parameters d and R_p should not be taken in their strict mechanistic sense, but rather as indicators of the integral corrosion behaviour of the interfacial layer. Of course, it is not possible to conclude in this work, whether the improvement of the effective corrosion performance corresponding to the addition of OVA actually derives from the presence of an adsorbed layer rather than on some modification of the passivating oxide layer. In addition to information regarding adsorbed OVA, our Raman results (Sect. 3.3) also show that the surface structure after corrosion in the OVA-containing SBF solution preserves the rutile structure and exhibits the presence of phosphate, as found in the pure SBF electrolyte.

3.2.3 *The system Ti/plasma*

In Fig. 9 we report the EIS spectra of anodised Ti in contact with the plasma, measured over a period of 63 h. The evolution of the OCP as a function of time—exhibiting a immediate ennobling reaching an asymptotic value of ca. 500 mV from an initial one of ca. −480 mV—is shown in Fig. 5c. The estimates of time-dependent passive film thickness d and resistance R_p are reported in Figs. 6c and

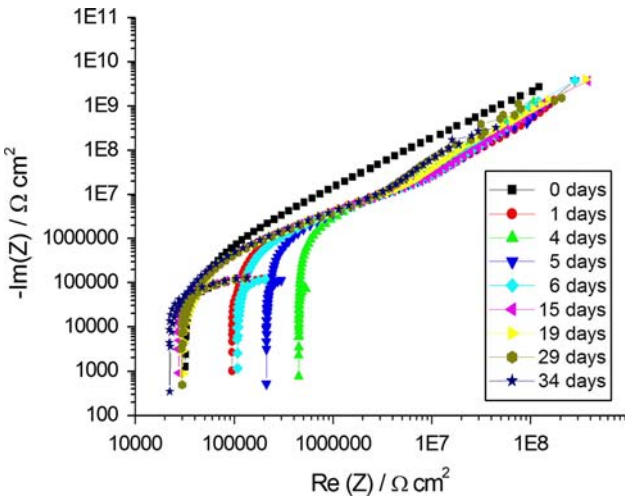

Fig. 8 EIS spectra of anodised Ti in contact with the SBF solution containing OVA

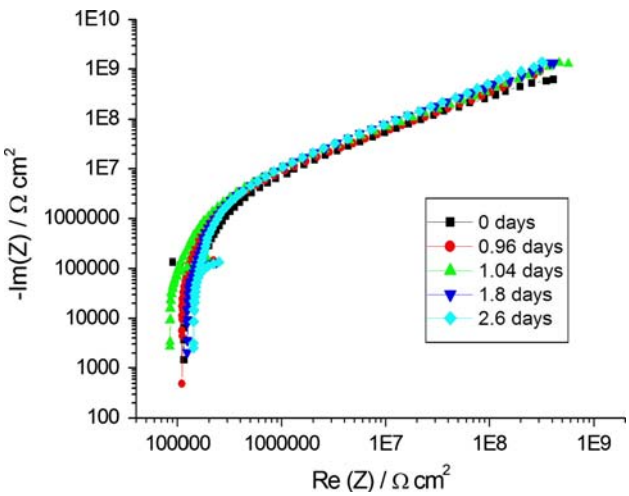

Fig. 9 EIS spectra of anodised Ti in contact with plasma

Table 3 Chief electrochemical parameters and their variation ranges for electrochemical corrosion experiments of Ti/TiO_2 systems exposed to environments relevant to dental applications

SYSTEM	OCP/V versus Ag/AgCl	Thickness (nm)	R_p ($M\Omega\ cm^2$)
SBF	−0.12 to 0.25	3–15	2–0.010
SBF OVA	ca. 0	3–2	2–0.003
Plasma	−0.48 to 0.50	5–10	1–10

7c. Approximately linear increases in d (ca. 5–10 nm) and R_p (ca. 1.2–10 $M\Omega\ cm^2$) were found. The initial thickness is higher and the initial resistance is significantly lower in the plasma solution than in SBF without and with OVA, possibly owing to an alteration of the oxide film in the biological fluid. During the immersion time, the film properties seem to improve slightly, but the corrosion resistance of anodised Ti in plasma was found to be remarkably lower than in the other SBF-based solutions studied. Of course, a systematic comparison of the results obtained in plasma, with respect to the cognate ones previously discussed in this work, can be made only for the comparatively limited exposure time allowed by the availability of human plasma. Nevertheless–in the relevant timeframe—the results are so dramatically different that we can regard them as significant. In view of a fundamental study of the actual biological response of Ti-based implants, it would be highly recommendable to extend a similar research to longer exposure times. The development of micro-cells, allowing a minimal consumption of human plasma will contribute strongly to this issue.

Again, definitive mechanistic conclusions regarding the oxide film developing in this extremely complex system can hardly be drawn. Nevertheless, Raman spectroscopy suggests that a complex adsorbed or incorporated protein film is present at the Ti surface; an accurate speciation is not feasible within the scope of the present research. It is worth noting that the effect of plasma proteins on the effective corrosion behaviour of the oxide interface is profoundly different from that of OVA and our results suggest the existence of some specific chemical effect on oxide film formation—possibly accompanied by its amorphisation—as it is known, in general, from the biomineralisation literature (e.g. [56] and references therein contained).

The chief electrochemical parameters and their variation ranges during the exposure experiments are reported in Table 3.

3.3 Surface Raman spectroscopy

The structure of the anodised Ti foils before and after exposure to the environments used in this study has been studied by surface Raman spectroscopy. In Fig. 10 we show a spectrum corresponding to the anodisation layer used in this research (2 V). For comparison, we also report a spectrum obtained with the same approach, but with a terminal voltage of 150 V. The TiO_2 film grown at 2 V exhibits faint bands corresponding to the rutile phase, the one formed at 150 V displays the anatase phase; both results are coherent with the literature (see, e.g., [27–30, 57]).

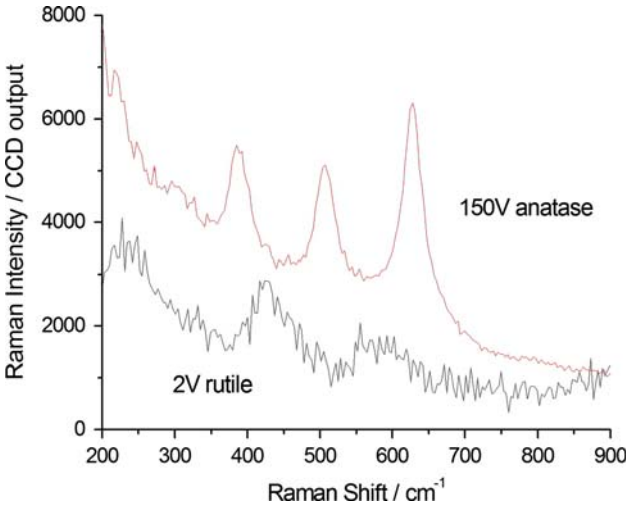

Fig. 10 Surface Raman spectra of as-anodised TiO_2 films formed on Ti at 2 and 150 V in 0.5 M H_2SO_4

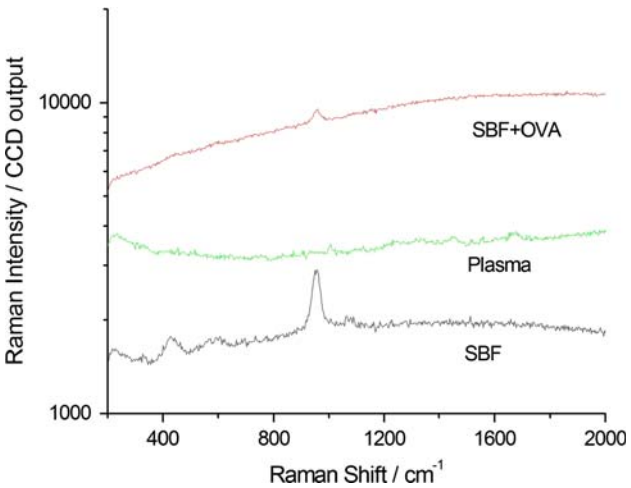

Fig. 11 Surface Raman spectra of TiO_2 films formed on Ti at 2 V in 0.5 M H_2SO_4 after exposure to the following solutions: (i) SBF, (ii) ovalbumin-containing SBF, (iii) human plasma

In Fig. 11 we report surface Raman spectra collected at the end of the corrosion experiments described in Sect. 3.2. One can notice that different vibrational features are found, corresponding to the three environments investigated.

(i) After exposure to the SBF solution, the rutile bands are accompanied by a new band at ca. 955 cm^{-1},

corresponding to PO_4^{3-} stretching (e.g. [58] and references therein contained). The presence of this band can be explained with the incorporation of phosphate into the outer, porous TiO_2 layer formed during the corrosion process; phosphate incorporation into TiO_2 layers has been reported previously, though in different contexts [59].

(ii) After immersion in the OVA-containing SBF solution, one can notice: (a) the development of a wide fluorescence band, that has been shown in the literature to be related to the presence of some types of so far poorly characterised organic films at the electrode surface (see, e.g. [60]); (b) a notable reduction of the absolute intensity of the rutile bands, possibly related to the presence of the fluorescent background; (c) the presence of the PO_4^{3-} stretching peak at ca. 955 cm^{-1}. This result suggests that the TiO_2 film grown in the relevant solution incorporates both phosphates and organics deriving from OVA.

(iii) The surface Raman spectrum recorded after immersion in plasma exhibits a different pattern: (a) a high fluorescent background—though not as high as that measured with the OVA-containing SBF solution; (b) a set of weak bands corresponding to several organic moieties, some of which aromatic (the low signal-to-noise ratio does not allow a conclusive band assignment); (c) no bands corresponding to known forms of crystalline TiO_2. Of course, this absence could be due to the high fluorescent background, nevertheless, growth of an amorphous porous top layer of TiO_2 incorporating species deriving from plasma still might be an acceptable explanation.

Of course, the structural differences found by surface Raman spectroscopy can be related to the differences in electrochemical behaviour, corresponding to different corrosion performance of the anodic films grown in the three solutions investigated.

Notwithstanding the drawback related to the estimated increase in corrosion rate, the oxide film thickness increase is liable to have a positive effect in clinical terms, relating to: (i) the immediate-loading issue; (ii) antibacterial properties related to limited amounts of released ions (i.e. below the osteoblast inhibition threshold), ensuring immunity to periimplant infection.

4 Conclusions

Anodised Ti exhibits a limited oxide growth and a systematic decrease of the film resistance, with the exception of the case of exposure to plasma, where a notable increase of film resistance is recorded, notwithstanding the comparatively limited thickness increase.

The EIS measurements performed in this research have demonstrated that the oxide film properties and attending corrosion resistance of the metal surface are strongly dependent on the environment and exposure time. Addition of ovalbumin to the SBF solution correlates with a notable increase of corrosion performance, possibly related to the adsorption of the protein onto the TiO_2 film. Comparison of the data concerning the SBF and plasma, reveals that the latter environment is remarkably more aggressive than the former. Surface Raman spectroscopy revealed that the degree of crystallinity of anodic films grown in the presence of organic species is reduced with respect to that of those formed during the exposure to SBF. Phosphate ends up incorporated from SBF solutions and entrapping of organics has been found to result from immersion in plasma.

References

1. S. Kothari, P.V. Halton, C.W. Douglas, J. Mater. Sci. **6**, 695 (1995)
2. T. Sawase, K. Hai, K. Yoshida, K. Baba, R. Hatada, M. Atsuta, J. Dent. **26**, 119 (1998)
3. Y.-T. Sul, C.B. Johansson, S. Petronis, A. Kroger, A. Weenerger, T. Albrektsson, Biomaterials **23**, 1809 (2002)
4. M. Wei, A.J. Ruys, M.V. Swain, B.K. Milthorpe, C.C. Sorrell, J. Mater. Sci.: Mater. Med. **16**, 101 (2005)
5. K. Elagli, M. Traisnel, H.F. Hildebrand, Electrochim. Acta **38**, 1769 (1993)
6. M. Long, H.J. Rack, Biomaterials **19**, 1621 (1998)
7. C. Aparicio, F.J. Gil, C. Fonseca, M. Barbosa, J.A. Planell, Biomaterials **23**, 263 (2003)
8. M. Svehla, P. Morberg, B. Zicat, W. Bruce, D. Sonnabend, W.R. Walsh, J. Biomed. Mater. Res. **51**, 15 (2000)
9. D. Buser, N. Broggini, M. Wieland, R.K. Schenk, A.J. Denzer, D.I. Cochran, B. Horfmann, A. Lussi, S.G. Steinemann, J. Dent. Res. **83**, 529 (2004)
10. V. Corsari, G. Giavaresi, M. Fini, P. Torricelli, M. Tschon, R. Chiesa, L. Chiusoli, A. salito, A. Volpert, R. Giardino, Biomaterials **26**, 4948 (2005)
11. D. Botticelli, T. Berglundh, L.G. Persson, J. Linde, J. Clin. Periodontol. **32**, 448 (2005)
12. S.-H. Seung-Han, R.R. Finões, C. Daraio, L.-H. Li-Han Chen, S. Jin, Biomaterials **26**, 4938 (2005)
13. A. Yamagami, Y. Yoshihara, F. Suwa, Int. J. Oral Maxillofac Impants **20**, 48 (2005)
14. J. Pan, D. Thierry, C. Laygraf, Electrochim. Acta **41**, 1143 (1996)
15. J.L. Gilbert, J. Biomed. Mater. Res. **40**, 233 (1998)
16. J.E.G. González, J.C. Mirza-Rosca, J. Electroanal. Chem. **471**, 109 (1999)
17. B. Grosgogeat, L. Reclaru, M. Lissac, F. Dalard, Biomaterials **20**, 933 (1999)
18. N. Ibriş, J.C. Mirza Rosca, J. Electroanal. Chem. **526**, 53 (2002)
19. M. Metikos, A. Kwokal, J. Pijac, Electrochim. Acta **24**, 3765 (2003)
20. A.M. Al-Mayouf, A.A. Al-Swayih, N.A. Al-Mobarak, A.S. Al-Jabab, Mat. Chem. Phys. **86**, 320 (2004)

21. I.C. Lavos-Valereto, S. Wolynec, I. Ramires, A.C. Guastaldi, I. Costa, J. Mater. Sci.: Mater. Med. **15**, 55 (2004)
22. C.E.B. Marino, L.H. Mascaro, J. Electroanal. Chem. **568**, 115 (2004)
23. D. Mareci, C. Bocanu, G. Nemtoi, D. Aelenei, J. Serb. Chem. Soc. **70**, 891 (2005)
24. A. Wennerberg, A. Ide-Ektassabi, S. Hatkamata, T. Sawase, C. Johansson, T. Albrektsson, A. Martinelli, U. Södervall, H. Oldelius, Clin. Oral. Implants Res. **15**, 505 (2004)
25. M. Pourbaix, Biomaterials **5**, 122 (1984)
26. K. Litner, J.W. Schultze, U. Stimming, J. Electrochem. Soc. **133**, 1561 (1986)
27. J.M. Bennett, E. Pelletier, G. Albrand, J.P. Borgogno, B. Lazarides, C.K. Carniglia, R.A. Schmell, T.H. Allen, T. Tuttle-Hart, K.H. Guenther, A. Saxer, Appl. Opt. **28**, 3303 (1989)
28. A. Felske, W.J. Plieth, Electrochim. Acta **34**, 75 (1989)
29. Lj.D Arsov, C. Kormann, W. Plieth, J. Electrochem. Soc. **138**, 2964 (1991)
30. U. Roland, E. Henssge, L. Sümmchen, R. Slazer, Zeitschr für Physik Chem **191**, 197 (1995)
31. J.F. McAleer, L.M. Peter, Faraday Discuss. R. Soc. Chem. **70**, 67 (1980)
32. W.F. Ho, C.P. Ju, J.H. Chern Lin, Biomaterials **20**, 2115 (1999)
33. J. Pjescic, S. Mentus, V. Komnenic, N. Blagojevic, J. Corros. Sci. Eng. **3**, 7 (2000)
34. C.E.B. Marino, E.M. Oliveira, R.C. Rocha-Filho, S.R. Biaggio, Corros. Sci. **43**, 1465 (2001)
35. V. Zwilling, M. Aucouturier, E. Darque-Ceretti, Electrochim. Acta **45**, 921 (1999)
36. J.-E. Sundgren, P. Bodö, I. Lundström, J. Colloid Interface Sci. **110**, 9 (1986)
37. L. Muszkat, L. Feigelson, L. Bir, K.A. Muszkat, J. Photochem. Photobiol. **60**, 32 (2001)
38. E. Jansson, P. Tengvall, Colloids Interfaces B **35**, 45 (2004)
39. J. Marsh, D. Gorse, Electrochim. Acta **43**, 659 (1998)
40. R. Godley, D. Starosvetsky, I. Gotman, J. Mater. Sci.: Mater. Med. **15**, 1073–1077 (2004)
41. K. Hitzig, W.J. Juttner, W. Lorenz, J. Paatsch, J. Electochem. Soc. **133**, 887 (1986)
42. F. Mansfeld, M.W. Kendig, J. Electrochem. Soc. **135**, 828 (1988)
43. E.P.M. van Westing, G.M. Ferrari, D.H. van der Weijde, J.H.W. de Wit, Corros. Sci. **34**, 937 (1993)
44. I.C. Lavos-Valereto, I. Costa, S. Wolynec, J. Biomed. Mater. Res. (Appl. Biomater.) **63**, 664 (2002)
45. J. Pan, D. Thierry, C. Leygraf, J. Biomed. Mater. Res. **28**, 113 (1994)
46. T. Ohtsuka, T. Otsuki, Corros. Sci. **40**, 951 (1998)
47. D.J. Blackwood, Electrochim. Acta **46**, 563 (2000)
48. R. Venugopalan, J.J. Weimer, M.A. Gorge, L.C. Lucas, Biomaterials **21**, 1669 (2000)
49. T.M. Silva, J.E. Rito, A.M.P. Simões, M.G.S. Ferreira, M. da Cunha Belo, K.G. Watkins, Electrochim. Acta **43**, 203 (1998)
50. G.C. Silva, C.S. Fuglvara, G. Tremiliosi Filho, P.T.A. Sumodjo, A.V. Benedetti, Electrochim. Acta **47**, 1875 (2002)
51. I. Sgura, B. Bozzini, Int. J. Non-Linear Mech. **40**, 557 (2005)
52. B. Bozzini, I. Sgura, Nonlinear Anal.: Real World Appl. **9**, 412 (2008)
53. B. Bozzini, G. Giovannelli, M. Boniardi, P.L. Cavallotti, Compos. Sci. Technol. **59**, 1579 (1999)
54. B. Bozzini, S. Maffi, L. D'Urzo, L. Peraldo Bicelli, Submitted to Corros. Rev.
55. B. Bozzini, G. Giovannelli, L. D'Urzo, in *Advanced technologies, research—development—application*, ed. by ARS (Vienna, 2006) p. 156
56. X.-Y. Guo, D.-P. Xu, Z.-H. Ding, W.-H. Su, Chin. Phys. Lett. **23**, 1645 (2006)
57. B. Bozzini, V. Romanello, C. Mele, Surf. Coat. Technol. **201**, 6267 (2007)
58. C.A. Borrás, R. Romagnoli, R.O. Lezna, Electrochim. Acta **45**, 1717 (2000)
59. B. Bozzini, B. Busson, G.P. De Gaudenzi, L. D'Urzo, C. Mele, A. Tedjeddine, J. Electroanal. Chem. **602**, 61 (2007)
60. B. Bozzini, S.A. Campbell, L. D'Urzo, Trans. IMF **85**, 212 (2007)